



First-principle investigations of nitrogen-, boron-, phosphorus-doped graphite electrodes for vanadium redox flow batteries

A. Xu, L. Shi, L. Zeng, T.S. Zhao*

HKUST Energy Institute, Department of Mechanical and Aerospace Engineering, The Hong Kong University of Science and Technology, Hong Kong, China



ARTICLE INFO

Article history:

Received 16 July 2018

Received in revised form

20 January 2019

Accepted 21 January 2019

Available online 25 January 2019

Keywords:

Vanadium redox flow battery

Density functional theory calculation

Heteroatom doping

Carbon electrode

ABSTRACT

An issue that limits the large-scale application of vanadium redox flow batteries (VRFBs) is their low power density, which is associated with the slow reaction kinetics of vanadium redox couples. To enhance the activities of the electrode toward vanadium redox couples, modifying carbon electrode surfaces with heteroatom doping is an effective strategy. In this work, we investigate the catalytic activity of nitrogen (N), boron (B) and phosphorus (P) doped graphite electrodes for VRFBs via density functional theory calculations. A layer of graphene is adopted to represent the surface of a graphite electrode. It is found that water adsorption is stronger with hydrogenated pyridinic N-doped and pyrrolic N-doped graphene than that of graphitic N-, B- and P-doped graphene, while the density of state of all the modified graphene remains metallic features. These results indicate good wettability and electronic conductivity of heteroatom doped graphite electrodes for VRFBs. To further evaluate their catalytic activity towards the V^{2+}/V^{3+} redox reaction, the metrics of energy difference between inner-sphere and outer-sphere adsorption modes for $V(H_2O)_6^{2+}$ and $V(H_2O)_6^{3+}$ are considered. An interesting finding is that for the P-doped graphene surface, the catalytic activity for both V^{2+} and V^{3+} ions can be significantly improved, suggesting a promising method for developing carbon electrodes for VRFBs.

© 2019 Elsevier Ltd. All rights reserved.

1. Introduction

Vanadium redox flow batteries (VRFBs) are energy storage devices which provide a promising solution to tackle challenges associated with the intermittent nature of solar energy and wind energy [1–3]. In VRFBs, electrolytes containing dissolved vanadium redox species flow through an electrochemical cell of porous carbon electrodes to lose or gain electrons [4–7]. The electrochemical reaction in VRFBs can be expressed as $VO_2^+ + 2H^+ + e^- \xrightleftharpoons{\text{charge}} VO^{2+} + H_2O$ at the positive electrode, and $V^{2+} \xrightleftharpoons{\text{charge}} V^{3+} + e^-$ at the negative electrode. The striking features of VRFBs include long lifetime, high energy efficiency, low maintenance cost, separately designed power and energy capacity, reduced crossover contamination, etc. However, one of the major barriers that limits the large-scale commercialization of VRFBs is their low power density, which is associated with the slow reaction kinetics of vanadium redox couples. An approach to overcoming power density limitation of VRFBs is to modify the

carbon electrode surface so that its electrochemical activities can be enhanced [8–11]. These surface treatments include structural modification, thermal treatment, acid treatment, metal doping, heteroatom doping, etc.

Heteroatom doping is a technique that introduces atoms of different elements, such as nitrogen (N), boron (B), phosphorus (P) and sulfur (S) into the lattice of carbon materials as heteroatom dopants [12,13]. This technique can effectively tune the intrinsic properties of carbon materials, and it has been widely used in many energy storage systems [14–16]. In VRFBs, the first attempt to utilize an N-doped carbon electrode may be attributed to Shao et al. [17]. They prepared mesoporous carbon electrode via a soft-template method and the nitrogen was doped by heat treating the electrode in NH_3 . The electrocatalytic kinetics and reversibility of VO^{2+}/VO_2^+ was found to be enhanced. They explained that N-doping facilitates the electron transfer on electrode/electrolyte interface for both oxidation and reduction process. Later, Wu et al. [18] developed N-doped graphite felt as the electrode material via hydrothermal ammoniated treatment. In addition to doping N into mesoporous carbon and graphite felt electrodes, Wang et al. [19] developed N-doped carbon nanotubes with graphite felt substrates as electrodes for VRFBs using chemical vapor deposition method.

* Corresponding author.

E-mail address: metzhao@ust.hk (T.S. Zhao).

They explained that the improved cell performance originated from the modified electronic properties and increased surface oxygen species of the carbon nanotubes as the result of N-doping. To identify the role of nitrogen species for the $\text{VO}^{2+}/\text{VO}_2^+$ couple reaction, Jin et al. [20] synthesized N-doped graphene sheets by annealing graphite oxide with urea. They proposed that the enhanced catalytic activity for $\text{VO}^{2+}/\text{VO}_2^+$ reaction resulted from the change of electron density and newly created localized states, which facilitated the adsorption of $\text{VO}^{2+}/\text{VO}_2^+$ ions on nitrogen dopant and conjugation of electron of reaction into these localized states. They further confirmed that not the nitrogen doping level but the nitrogen type in the graphene sheets determined the catalytic activity, and the quaternary-N species provide more active sites and a catalyst for the $\text{VO}^{2+}/\text{VO}_2^+$ redox reaction. Shi et al. [21] further proved that the quaternary-N plays the main role in accelerating the $\text{VO}^{2+}/\text{VO}_2^+$ redox reactions. Their graphene nano-sheets electrodes were prepared through hydrothermal reaction with urea as the nitrogen source, and the nitrogen species could be turned by controlling the hydrothermal reaction time.

The above studies focused on utilizing N-doped carbon

electrodes in VRFBs, while efforts on adopting B- and P-doped carbon electrodes in VRFBs have also been made. For example, Shi et al. [22] prepared B- or N- mono-doped carbon nanofiber electrodes by electrospinning method. Improved electrochemical performance for the $\text{VO}^{2+}/\text{VO}_2^+$ redox reaction was observed. In addition, they investigated B and N co-doped carbon nanofiber electrodes with separated case and bonded case. They concluded that not the total amount of incorporated B and N but how the B and N are incorporated into carbon nanostructures determines the catalytic activity toward $\text{VO}^{2+}/\text{VO}_2^+$ redox reaction. He et al. [23] prepared N-, P-, co-doped carbon microsphere electrodes by hydrothermal treatment followed by calcination with $(\text{NH}_4)_2\text{HPO}_4$ as N and P sources. The superior electrochemical performance was ascribed to the increased total number of heteroatoms as active sites and synergistic effect of N- and P- co-doping.

Despite numerous experimental investigations on the heteroatom doping in VRFBs, there lacks comprehensive comparison of heteroatom-doped carbon electrodes with different elements. In this work, we present first-principle investigations on the adsorption-desorption behavior of aqueous $\text{V}^{2+}/\text{V}^{3+}$ redox species on the basal plane of nitrogen, boron and phosphorus doped graphite electrode surface. Because graphite consists of single graphene layers connected via van der Waals force, graphene layer is chosen to represent the basal plane of graphite electrode for simplicity [24–26]. Our computational results promote the understanding of $\text{V}^{2+}/\text{V}^{3+}$ redox reaction and provide in-depth insight into the heteroatom doping of carbon electrodes in VRFBs.

2. Computational details

DFT computations were performed based on plane-wave

Table 1
Structure parameters of pristine graphene and N-, B-, P-doped graphene.

	<i>a</i> (Å)	<i>b</i> (Å)
pristine graphene	9.8564	12.8236
graphitic N-doped graphene	9.8526	12.8130
hydrogenated pyridinic N-doped graphene	9.8654	12.8353
hydrogenated pyrrolic N-doped graphene	9.8254	12.9431
graphitic B-doped graphene	9.8999	12.8747
graphitic P-doped graphene	9.8942	12.8672

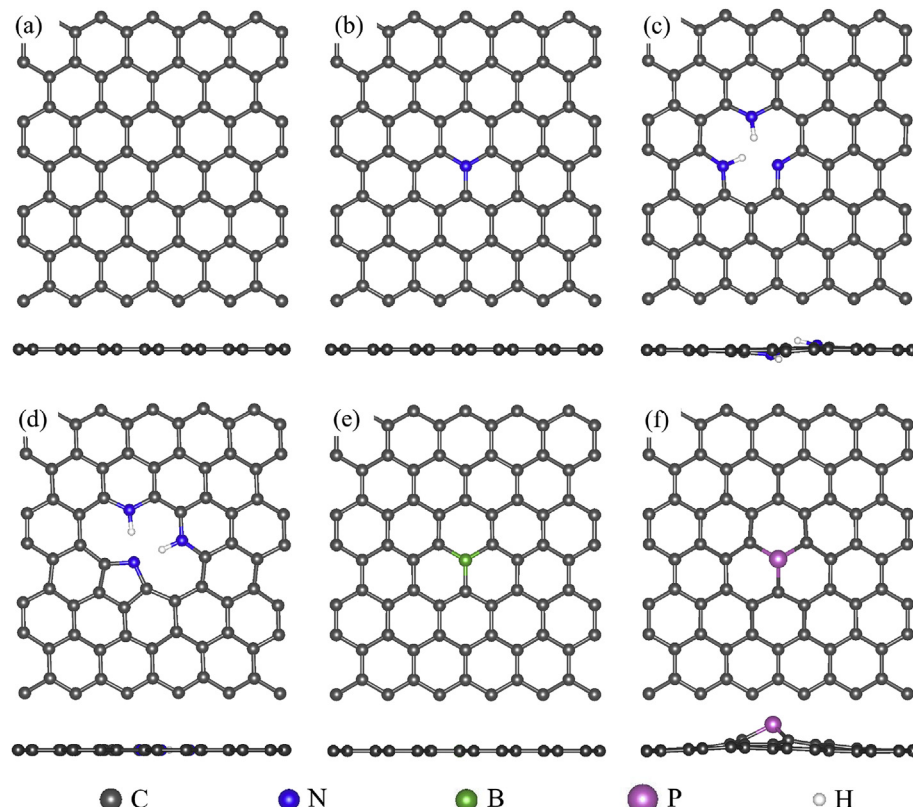


Fig. 1. Top and side view of the atomic structure of (a) pristine graphene, (b) graphitic N-doped graphene, (c) hydrogenated pyridinic N-doped graphene, (d) hydrogenated pyrrolic N-doped graphene, (e) graphitic B-doped graphene, and (f) graphitic P-doped graphene.

technique implemented in the ABINIT software package (version 8.6.3) [27–31]. Projector-augmented plane wave (PAW) pseudo-potentials were used to describe the ion-electron interactions [32]. A generalized gradient approximation (GGA) expressed by the Perdew-Burke-Ernzerhof (PBE) functional was adopted to treat the exchange-correlation functional [33]. To describe the van der Waals interaction, Grimme's D2 correction was adopted [34]. The cutoff energy for the plane-wave basis was set to be 20 Ha. For geometrical optimization, the force tolerance was set to be 0.02 eV/Å. A uniform compensating background was added to restore the charge neutrality.

The graphene substrate expands along the *a* and *b* directions ($a \approx 9.9$ Å, $b \approx 12.8$ Å, detailed values of *a* and *b* for each graphene substrate is given in Table 1); the vacuum space in the *c* direction was set to be 20 Å to avoid any interlayer interactions. Integrations over the Brillouin zones were sampled with a $3 \times 2 \times 1$ mesh of uniformly spaced *k* points such that the *k*-point mesh is less than 0.05 Å⁻¹. For density of states (DOS) calculation, a denser *k*-point mesh less than 0.02 Å⁻¹ was used. To calculate the water adsorption energy, a cubic supercell of length 10 Å containing a single H₂O molecule was constructed and only the Gamma point was sampled in the Brillouin zone. The adsorption energy is then calculated as $E_{\text{ads}} = E_{\text{total}} - E_{\text{substrate}} - E_{\text{H}_2\text{O}}$, where E_{total} , $E_{\text{substrate}}$ and $E_{\text{H}_2\text{O}}$ represent the energy of the total system, the graphene substrate and the water adsorbate, respectively. To prepare the hydration shell geometry of aqueous V(H₂O)₆²⁺ and V(H₂O)₆³⁺, a cubic supercell of length 20 Å containing one V atom and six H₂O molecules was constructed, and only the Gamma point was sampled in

the Brillouin zone.

3. Results and discussion

According to previous investigations of N-doped, B-doped and P-doped graphene, there are three kinds of in-plane N configurations (i.e., graphitic N-dope, pyridinic N-dope, and pyrrolic N-dope), one kind of in-plane B configuration (i.e., graphitic B-dope) and one kind of in-plane P configuration (i.e., graphitic P-dope) in the lattice of graphene [13,35]. The atomic structures in this study are shown in Fig. 1. The graphitic N-, B-, and P-doped graphene is built by replacing one C atom with a N, B, and P atom, respectively. In the graphitic N- and B-doped graphene, all atoms are in one plane; while in the graphitic P-doped graphene, the P atom protrudes out of the graphene plane. For pyridinic N-doped and pyrrolic N-doped graphene, we found that for the cases without hydrogenation or with only one hydrogen atom included, the interaction between graphene substrate and water molecules is so strong that the O–H bond in water molecules will be torn apart and new N–H bond will be formed. This phenomenon indicates that bare pyridinic N-doped or pyrrolic N-doped graphene is highly unstable in aqueous environment and will be transferred into hydrogenated configurations quickly. Thus, we adopted hydrogenated configurations with two hydrogen atoms in our computations. For the hydrogenated pyridinic N-doped graphene, the H atoms protrude out of the graphene plane, as shown in Fig. S1. This configuration is more stable compare to the configuration where all atoms sits in one plane, since its total energy difference is 0.158 eV

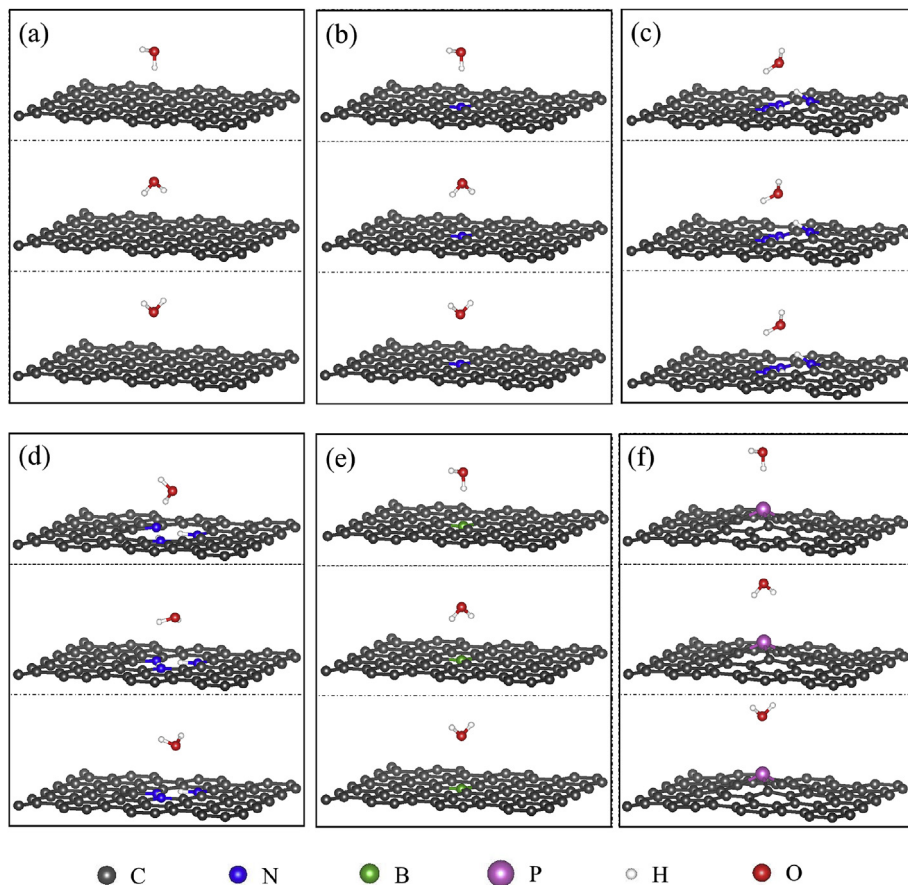


Fig. 2. Water adsorption configurations on (a) pristine graphene, (b) graphitic N-doped graphene, (c) hydrogenated pyridinic N-doped graphene, (d) hydrogenated pyrrolic N-doped graphene, (e) graphitic B-doped graphene, and (f) graphitic P-doped graphene.

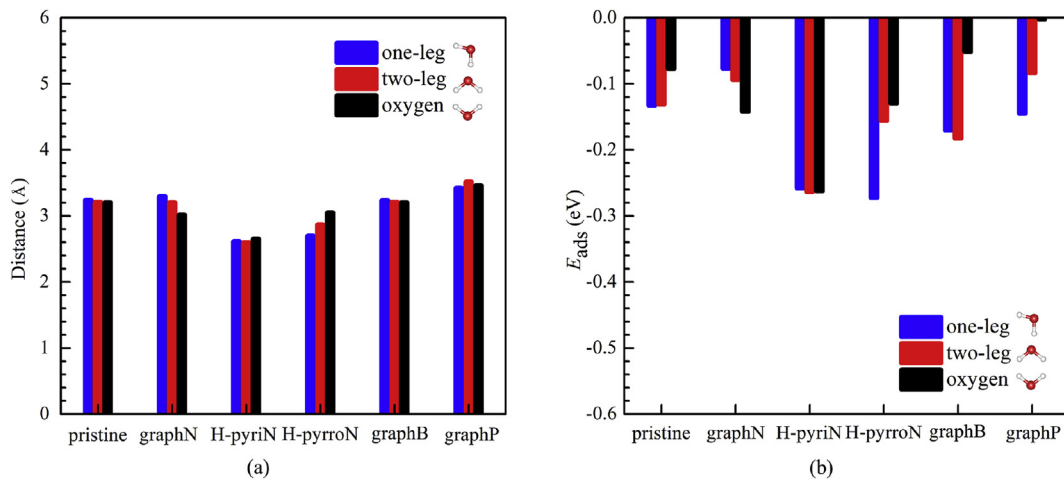


Fig. 3. (a) Water adsorption energies and (b) the distances between water and graphene surfaces.

lower. The electron distribution map for graphene doped with different elements are provided in Fig. S2.

We first calculate the water adsorption energies and the distances between H_2O and different graphene surfaces to evaluate the wettability of carbon electrode surface. The detailed adsorption configurations are given in Fig. 2. Three adsorption modes were considered in our computations [36–38]. From Fig. 3, we can see that the adsorption energy for isolated H_2O molecule on monolayer pristine graphene is around 0.13 eV, which is consistent with previous works [38–40]. The absolute values of all the adsorption energies are smaller than 0.3 eV; the optimized distances between the oxygen atom of H_2O molecule and graphene surfaces are all larger than 2.5 Å (for the case of graphitic P-doped graphene, we calculate the distance between oxygen atom and phosphorus atom since the basal graphene plane is distorted). In addition, for the hydrogenated pyridinic N-doped and pyrrolic N-doped graphene,

the water adsorption energies are larger, and the distances between water and graphene surfaces are shorter. On the other hand, the water adsorption mode is still physisorption rather than chemisorption as indicated in Fig. 3. Overall, these results indicate the interactions between H_2O and graphene surfaces are mainly weak van der Waals forces. We then calculate the density of states (DOS) for different graphene surfaces. As shown in Fig. 4, all the heteroatom doped surfaces under consideration can preserve their metallic features well, which ensures the high electronic conductivity of the carbon electrode in VRFBs.

The optimized first coordination sphere of aqueous $V(H_2O)_6^{2+}$ and $V(H_2O)_6^{3+}$ and their corresponding structure parameters are given in Fig. 5 and Table 2, respectively. Fig. 6 illustrates the adsorption modes of V^{2+} and V^{3+} ions on pristine graphene. Here, we consider one inner-sphere adsorption mode and three outer-sphere adsorption modes. The inner-sphere adsorption mode is built by placing one water molecule into the second coordination

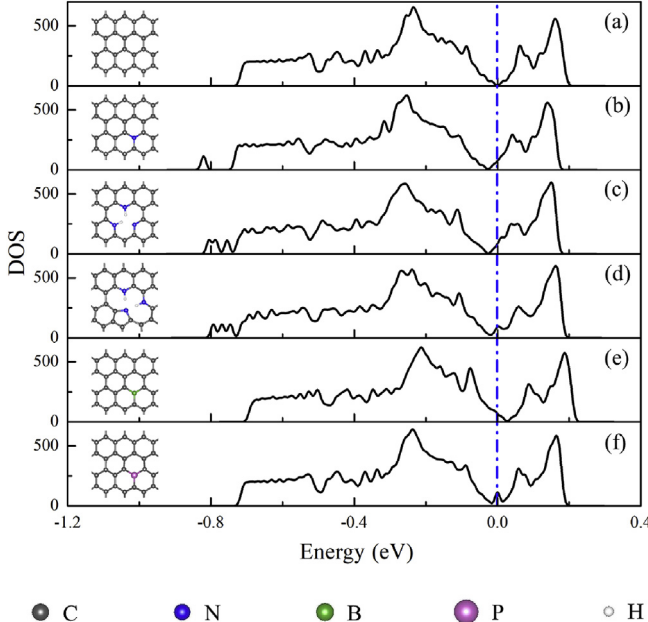


Fig. 4. Density of states of (a) pristine graphene, (b) graphitic N-doped graphene, (c) hydrogenated pyridinic N-doped graphene, (d) hydrogenated pyrrolic N-doped graphene, (e) graphitic B-doped graphene, and (f) graphitic P-doped graphene.

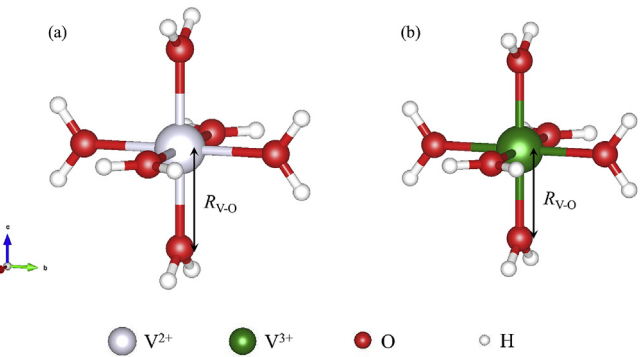


Fig. 5. First coordination sphere of aqueous vanadium ions: (a) $V(H_2O)_6^{2+}$; (b) $V(H_2O)_6^{3+}$.

Table 2
Structural parameters of $V(H_2O)_6^{2+}$ and $V(H_2O)_6^{3+}$.

Method	$V^{2+} (R_{V-O}, \text{Å})$	$V^{3+} (R_{V-O}, \text{Å})$
Present	2.124	2.039
CPMD [44]	2.23	2.10
B3LYP [42]	2.21	2.09
HF [45]	2.20	2.06
XRD [46,47]	2.13	2.00

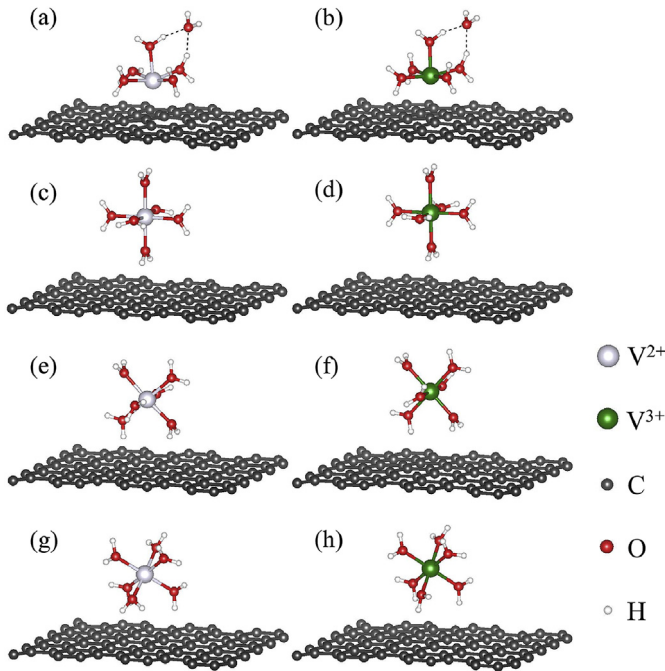


Fig. 6. Adsorption modes of $\text{V}(\text{H}_2\text{O})_6^{2+}$ and $\text{V}(\text{H}_2\text{O})_6^{3+}$ on pristine graphene surfaces.

sphere; the three outer-sphere adsorption modes are built based on the T_h symmetry of the $\text{V}(\text{H}_2\text{O})_6^{2+}$ and $\text{V}(\text{H}_2\text{O})_6^{3+}$. Hirshfeld charge analysis [41] and V–O bond lengths for isolated and adsorbed $\text{V}(\text{H}_2\text{O})_6^{2+}/\text{V}(\text{H}_2\text{O})_6^{3+}$ on pristine graphene surface are provided in Figs. S3–S12. Similar adsorption modes of $\text{V}(\text{H}_2\text{O})_6^{2+}$ and $\text{V}(\text{H}_2\text{O})_6^{3+}$ adsorbed on N-, B-, and P-doped graphene surfaces are considered in the following discussion.

The charge transfer for V^{2+} ions and V^{3+} ions adsorbed on pristine graphene surfaces are shown in Figs. 7 and 8, respectively. From the charge transfer map, we can clearly observe that the charge transfer between vanadium ions and graphene surfaces are mainly conducted via inner-sphere adsorption mode. Since outer-sphere modes mainly exist in bulk electrolyte solution and the redox reaction of $\text{V}^{2+}/\text{V}^{3+}$ is a simple one-electron transfer process,

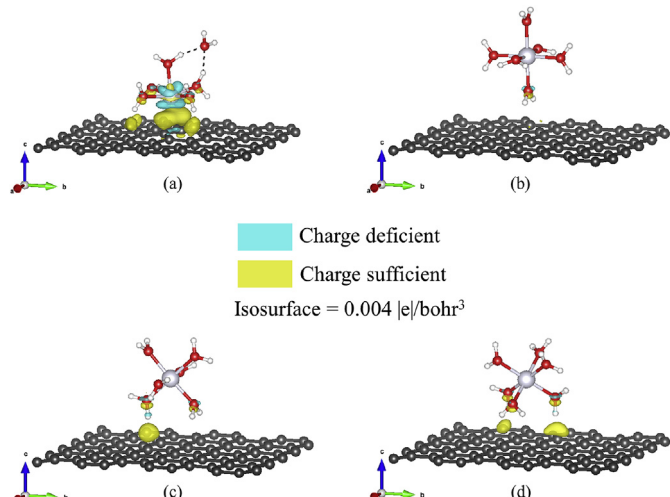


Fig. 7. Charge transfer of V^{2+} ions adsorbed on the pristine graphene surfaces.

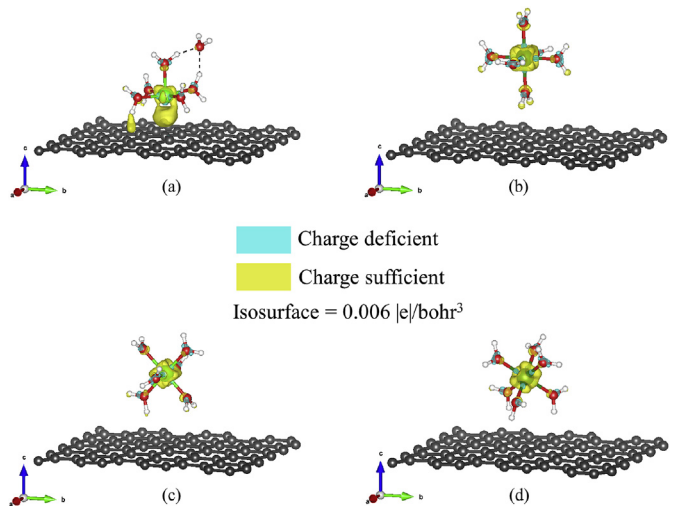


Fig. 8. Charge transfer of V^{3+} ions adsorbed on the pristine graphene surfaces.

the stabilization of the inner-sphere adsorption mode will directly contribute to the reaction kinetics and enhance the catalytic activity [9,42,43]. Thus, in the following, we will adopt the metrics of $\Delta E = E_{\text{inner}} - E_{\text{outer}}$ to quantify the ability of the graphene surfaces to facilitate the transformation of $\text{V}^{2+}/\text{V}^{3+}$ adsorption modes from the outer-sphere mode to the inner-sphere mode.

The energy difference between the inner-sphere adsorption and outer-sphere adsorption modes for $\text{V}^{2+}/\text{V}^{3+}$ ions on different kinds of surfaces are shown in Fig. 9. From the results, we can see that on pristine graphene surface, the formation of inner-sphere adsorption mode for V^{3+} ions are harder than that for V^{2+} ions, which is consistent with the experimental observation that V^{3+} ions show sluggish reaction kinetics. It is also found that graphitic N-doped graphene will slightly facilitate the formation of inner-sphere mode for V^{2+} , while pyridinic N-doped graphene surface will enhance its activity towards V^{3+} . This indicates that different kinds of N atom doping may play different roles in the redox reaction of $\text{V}^{2+}/\text{V}^{3+}$. For B-doped graphene surface, its catalytic activity towards V^{3+} ions is more prominent. An interesting finding is that for P-doped

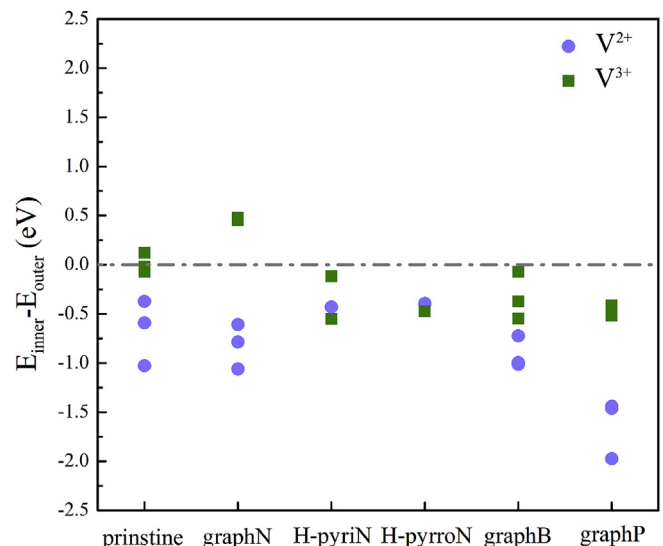


Fig. 9. The energy difference between the inner-sphere and outer-sphere adsorption modes for V^{2+} and V^{3+} ions on different graphene surfaces.

graphene surface, the catalytic activity towards both V^{2+} and V^{3+} ions can be significantly improved. Although limited experimental efforts have been focused on the P-doped graphite as the electrodes for VRFBs, here our theoretical work suggests a promising method for developing graphite electrodes for VRFBs.

4. Conclusions

In this work, we provide a comprehensive exploration on the feasibility of N-, B-, and P-doped graphite as electrodes for VRFBs via density functional theory calculations. The main findings are summarized as follows:

1. The water interaction is stronger with hydrogenated pyridinic N-doped and pyrrolic N-doped graphene than that of graphitic N-, B- and P-doped graphene, while the density of state of all the modified graphene remains metallic features. These indicate the good wettability and electronic conductivity of heteroatom doped graphite electrodes for VRFBs.
2. Graphitic N-doped graphene will slightly facilitate the formation of inner-sphere mode for V^{2+} , while pyridinic N-doped graphene surface will enhance its activity towards V^{3+} . For B-doped graphene surface, its catalytic activity towards V^{3+} ions is more prominent. For P-doped graphene surface, its catalytic activity towards both V^{2+} and V^{3+} ions can be significantly improved. Future research efforts may be focused on utilizing P-doped graphite as electrodes for VRFBs.

Acknowledgement

The work described in this paper was fully supported by a grant from the Research Grant Council of the Hong Kong Special Administrative Region, China (Project No. T23-601/17-R).

Appendix A. Supplementary data

Supplementary data to this article can be found online at <https://doi.org/10.1016/j.electacta.2019.01.109>.

References

- [1] M.L. Perry, A.Z. Weber, Advanced redox-flow batteries: a perspective, *J. Electrochem. Soc.* 163 (1) (2016) A5064–A5067.
- [2] G.L. Soloveichik, Flow batteries: current status and trends, *Chem. Rev.* 115 (20) (2015) 11533–11558.
- [3] C. Ding, H. Zhang, X. Li, T. Liu, F. Xing, Vanadium flow battery for energy storage: prospects and challenges, *J. Phys. Chem. Lett.* 4 (8) (2013) 1281–1294.
- [4] Q. Xu, T. Zhao, Fundamental models for flow batteries, *Prog. Energy Combust. Sci.* 49 (2015) 40–58.
- [5] Q. Zheng, X. Li, Y. Cheng, G. Ning, F. Xing, H. Zhang, Development and perspective in vanadium flow battery modeling, *Appl. Energy* 132 (2014) 254–266.
- [6] P. Alotto, M. Guarneri, F. Moro, Redox flow batteries for the storage of renewable energy: a review, *Renew. Sustain. Energy Rev.* 29 (2014) 325–335.
- [7] A.Z. Weber, M.M. Mench, J.P. Meyers, P.N. Ross, J.T. Gostick, Q. Liu, Redox flow batteries: a review, *J. Appl. Electrochem.* 41 (10) (2011) 1137.
- [8] M. Park, J. Ryu, W. Wang, J. Cho, Material design and engineering of next-generation flow-battery technologies, *Nat. Rev. Mater.* 2 (1) (2017) 16080.
- [9] K.J. Kim, M.-S. Park, Y.-J. Kim, J.H. Kim, S.X. Dou, M. Skylas-Kazacos, A technology review of electrodes and reaction mechanisms in vanadium redox flow batteries, *J. Mater. Chem. 3* (33) (2015) 16913–16933.
- [10] M. Chakrabarti, N. Brandon, S. Hajimolana, F. Tariq, V. Yusif, M. Hashim, M. Hussain, C. Low, P. Aravind, Application of carbon materials in redox flow batteries, *J. Power Sources* 253 (2014) 150–166.
- [11] A. Parasuraman, T.M. Lim, C. Menictas, M. Skylas-Kazacos, Review of material research and development for vanadium redox flow battery applications, *Electrochim. Acta* 101 (2013) 27–40.
- [12] J.P. Paraknowitsch, A. Thomas, Doping carbons beyond nitrogen: an overview of advanced heteroatom doped carbons with boron, sulphur and phosphorus for energy applications, *Energy Environ. Sci.* 6 (10) (2013) 2839–2855.
- [13] X. Wang, G. Sun, P. Routh, D.-H. Kim, W. Huang, P. Chen, Heteroatom-doped graphene materials: syntheses, properties and applications, *Chem. Soc. Rev.* 43 (20) (2014) 7067–7098.
- [14] L. Shi, T. Zhao, Recent advances in inorganic 2D materials and their applications in lithium and sodium batteries, *J. Mater. Chem. A* 5 (8) (2017) 3735–3758.
- [15] X. Wang, G. Shi, An introduction to the chemistry of graphene, *Phys. Chem. Chem. Phys.* 17 (43) (2015) 28484–28504.
- [16] C. Xu, B. Xu, Y. Gu, Z. Xiong, J. Sun, X. Zhao, Graphene-based electrodes for electrochemical energy storage, *Energy Environ. Sci.* 6 (5) (2013) 1388–1414.
- [17] Y. Shao, X. Wang, M. Engelhard, C. Wang, S. Dai, J. Liu, Z. Yang, Y. Lin, Nitrogen-doped mesoporous carbon for energy storage in vanadium redox flow batteries, *J. Power Sources* 195 (13) (2010) 4375–4379.
- [18] T. Wu, K. Huang, S. Liu, S. Zhuang, D. Fang, S. Li, D. Lu, A. Su, Hydrothermal ammoniated treatment of PAN-graphite felt for vanadium redox flow battery, *J. Solid State Electrochem.* 16 (2) (2012) 579–585.
- [19] S. Wang, X. Zhao, T. Cochell, A. Manthiram, Nitrogen-doped carbon nanotube/graphite felts as advanced electrode materials for vanadium redox flow batteries, *J. Phys. Chem. Lett.* 3 (16) (2012) 2164–2167.
- [20] J. Jin, X. Fu, Q. Liu, Y. Liu, Z. Wei, K. Niu, J. Zhang, Identifying the active site in nitrogen-doped graphene for the VO^{2+}/vo_2^+ redox reaction, *ACS Nano* 7 (6) (2013) 4764–4773.
- [21] L. Shi, S. Liu, Z. He, J. Shen, Nitrogen-doped graphene: effects of nitrogen species on the properties of the vanadium redox flow battery, *Electrochim. Acta* 138 (2014) 93–100.
- [22] L. Shi, S. Liu, Z. He, H. Yuan, J. Shen, Synthesis of boron and nitrogen co-doped carbon nanofiber as efficient metal-free electrocatalyst for the VO^{2+}/vo_2^+ redox reaction, *Electrochim. Acta* 178 (2015) 748–757.
- [23] Z. He, Y. Jiang, Y. Wei, C. Zhao, F. Jiang, L. Li, H. Zhou, W. Meng, L. Wang, L. Dai, N. P co-doped carbon microsphere as superior electrocatalyst for VO^{2+}/vo_2^+ redox reaction, *Electrochim. Acta* 259 (2018) 122–130.
- [24] H. Johll, H.C. Kang, E.S. Tok, Density functional theory study of Fe, Co, and Ni adatoms and dimers adsorbed on graphene, *Phys. Rev. B* 79 (24) (2009) 245416.
- [25] J. Ma, A. Michaelides, D. Alfe, L. Schimka, G. Kresse, E. Wang, Adsorption and diffusion of water on graphene from first principles, *Phys. Rev. B* 84 (3) (2011) 033402.
- [26] A. Ambrosetti, P. Silvestrelli, Adsorption of rare-gas atoms and water on graphite and graphene by van der Waals-corrected density functional theory, *J. Phys. Chem. C* 115 (9) (2011) 3695–3702.
- [27] M. Torrent, F. Jollet, F. Bottin, G. Zérah, X. Gonze, Implementation of the projector augmented-wave method in the ABINIT code: application to the study of iron under pressure, *Comput. Mater. Sci.* 42 (2) (2008) 337–351.
- [28] M.A. Marques, M.J. Oliveira, T. Burnus, Libxc: a library of exchange and correlation functionals for density functional theory, *Comput. Phys. Commun.* 183 (10) (2012) 2272–2281.
- [29] X. Gonze, F. Jollet, F.A. Araujo, D. Adams, B. Amadon, T. Appelcourt, C. Audouze, J.-M. Beuken, J. Bieder, A. Bokhanchuk, et al., Recent developments in the ABINIT software package, *Comput. Phys. Commun.* 205 (2016) 106–131.
- [30] X. Gonze, B. Amadon, P.-M. Anglade, J.-M. Beuken, F. Bottin, P. Boulanger, F. Bruneval, D. Caliste, R. Caracas, M. Côté, et al., ABINIT: first-principles approach to material and nanosystem properties, *Comput. Phys. Commun.* 180 (12) (2009) 2582–2615.
- [31] X. Gonze, A brief introduction to the ABINIT software package, *Z. Krist.-Cryst. Mater.* 220 (5/6) (2005) 558–562.
- [32] P.E. Blöchl, Projector augmented-wave method, *Phys. Rev. B* 50 (24) (1994) 17953.
- [33] J.P. Perdew, M. Ernzerhof, K. Burke, Rationale for mixing exact exchange with density functional approximations, *J. Chem. Phys.* 105 (22) (1996) 9982–9985.
- [34] S. Grimme, Semiempirical GGA-type density functional constructed with a long-range dispersion correction, *J. Comput. Chem.* 27 (15) (2006) 1787–1799.
- [35] Y. Jing, Z. Zhou, Computational insights into oxygen reduction reaction and initial $Li_{2}O_2$ nucleation on pristine and N-Doped graphene in $Li-O_2$ batteries, *ACS Catal.* 5 (7) (2015) 4309–4317.
- [36] I. Hamada, Adsorption of water on graphene: a van der Waals density functional study, *Phys. Rev. B* 86 (19) (2012) 195436.
- [37] A. Ashraf, Y. Wu, M.C. Wang, K. Yong, T. Sun, Y. Jing, R.T. Haasch, N.R. Aluru, S. Nam, Doping-induced tunable wettability and adhesion of graphene, *Nano Lett.* 16 (7) (2016) 4708–4712.
- [38] G. Hong, Y. Han, T.M. Schützis, Y. Wang, Y. Pan, M. Hu, J. Jie, C.S. Sharma, U. Muler, D. Poulikakos, On the mechanism of hydrophilicity of graphene, *Nano Lett.* 16 (7) (2016) 4447–4453.
- [39] L. Shi, A. Xu, G. Chen, T. Zhao, Theoretical understanding of mechanisms of proton exchange membranes made of 2D crystals with ultrahigh selectivity, *J. Phys. Chem. Lett.* 8 (18) (2017) 4354–4361.
- [40] G. Levita, P. Restuccia, M. Righi, Graphene and MoS_2 interacting with water: a comparison by ab initio calculations, *Carbon* 107 (2016) 878–884.
- [41] F. Hirshfeld, Bonded-atom fragments for describing molecular charge densities, *Theor. Chim. Acta* 44 (2) (1977) 129–138.
- [42] F. Sepehr, S.J. Paddison, The solvation structure and thermodynamics of aqueous vanadium cations, *Chem. Phys. Lett.* 585 (2013) 53–58.
- [43] Z. Jiang, K. Klyukin, V. Alexandrov, First-principles study of adsorption–desorption kinetics of aqueous V^{2+}/V^{3+} redox species on graphite

- in a vanadium redox flow battery, *Phys. Chem. Chem. Phys.* 19 (23) (2017) 14897–14901.
- [44] Z. Jiang, K. Klyukin, V. Alexandrov, Structure, hydrolysis, and diffusion of aqueous vanadium ions from Car-Parrinello molecular dynamics, *J. Chem. Phys.* 145 (11) (2016) 114303.
- [45] R. Aakesson, L.G. Pettersson, M. Sandstroem, U. Wahlgren, Ligand field effects in the hydrated divalent and trivalent metal ions of the first and second transition periods, *J. Am. Chem. Soc.* 116 (19) (1994) 8691–8704.
- [46] F.A. Cotton, L.R. Falvello, R. Llusar, E. Libby, C.A. Murillo, W. Schwotzer, Synthesis and characterization of four vanadium (II) compounds, including vanadium (II) sulfate hexahydrate and vanadium (II) saccharinates, *Inorg. Chem.* 25 (19) (1986) 3423–3428.
- [47] F.A. Cotton, C.K. Fair, G.E. Lewis, G.N. Mott, F.K. Ross, A.J. Schultz, J.M. Williams, Precise structural characterizations of the hexaaquovanadium (III) and diaquaohydrogen ions. X-ray and neutron diffraction studies of $[V(H_2O)_6][H_5O_2](CF_3SO_3)_4$, *J. Am. Chem. Soc.* 106 (18) (1984) 5319–5323.